Unexpected linkage isomerism in chiral tetranuclear grids

Isabel N. Hegarty[a], Hannah L. Dalton[a], Adam F. Henwood[a], Chris S. Hawes[b] and Thorfinnur Gunnlaugsson[*,a]

[a]School of Chemistry and Trinity Biomedical Science Institute, Trinity College Dublin,

Dublin 2, Ireland.

Supporting Information

Experimental

Materials and Methods

All reagents, solvents and starting materials were purchased from Sigma-Aldrich, Merck or Fisher Scientific, were of reagent grade or better, and were used as received. Mass spectra were acquired using a Micromass time of flight mass spectrometer (tof), interfaced to a Waters 2690 HPLC. The instrument was operated in positive or negative mode as required. Leucine Enkephalin was used as an internal lock mass. Elemental analyses were carried out at the Microanalytical Laboratory, School of Chemistry and Chemical Biology, University College Dublin and Chemistry Department, Maynooth University, Kildare. NMR data were recorded in commercially available deuterated solvents on a Bruker Avance II 600MHz spectrometer which operates at 600 MHz for ^{1}H and 150 MHz for ^{13}C resonances, or a Bruker Avance III spectrometer which operates at 400.13 MHz for ^{1}H NMR and 100.6 MHz for ^{13}C NMR. Tetramethylsilane (TMS) was used as an internal standard and shifts were referenced relative to the internal solvent signals with chemical shifts expressed in parts per million (ppm / δ). Infrared spectra were recorded on a Perkin Elmer Spectrum 100 FTIR spectrometer with universal ATR sampling accessory, in the range 4000 – 550 cm^{-1}. Cyclic voltammetry (CV) measurements were performed on an Electrochemical Analyzer potentiostat model 600D from CH Instruments with a PC controlled electrochemical workstation. Solutions for cyclic voltammetry were prepared in HPLC grade MeCN, which was dried using an in-house solvent purification system. A minimum volume of solvent (*ca.* 2–3 mL) was used. Pt wires were used as the pseudoreference electrode and the counter electrode, while an Au disk electrode was used for the working electrode. Both before and after the experiments, the Au disk electrode was cleaned by polishing the surface in an ethanol slurry of abrasive powder (gamma alumina powder, 0.05 micron, CH Instruments), before sonicating in ethanol, washing with acetone, water, and finally ethanol, and then drying. The electrochemical cell consisted of a glass vessel (*ca.* 40 mL) covered with a plastic lid and drilled with four holes: one for each electrode, and

one for nitrogen purging. The vessel was sealed with parafilm to ensure minimal oxygen contamination. Tetra(n-butyl)ammoniumhexafluorophosphate (TBAPF$_6$; *ca*. 0.1 M in MeCN) was used as the supporting electrolyte, with the solution degassed by vigorous bubbling for about 10 min prior to scanning the blank sample to ensure a clean background. Small quantities of sample were then added in portions, and then the mixture degassed and scanned. This process was repeated until an adequate signal-to-background ratio became apparent. The measurements in the appropriate electrochemical windows were then carried out, at scan rates of 0.1 and 1 V s^{-1}. At the end of each experiment, ferrocene was added as an internal reference, and then the scans were repeated, again at 0.1 and 1 V s^{-1}. Estimated error: ±30 mV. The redox potentials are reported relative to the ferrocenium/ferrocene (Fc$^+$/Fc) redox couple.
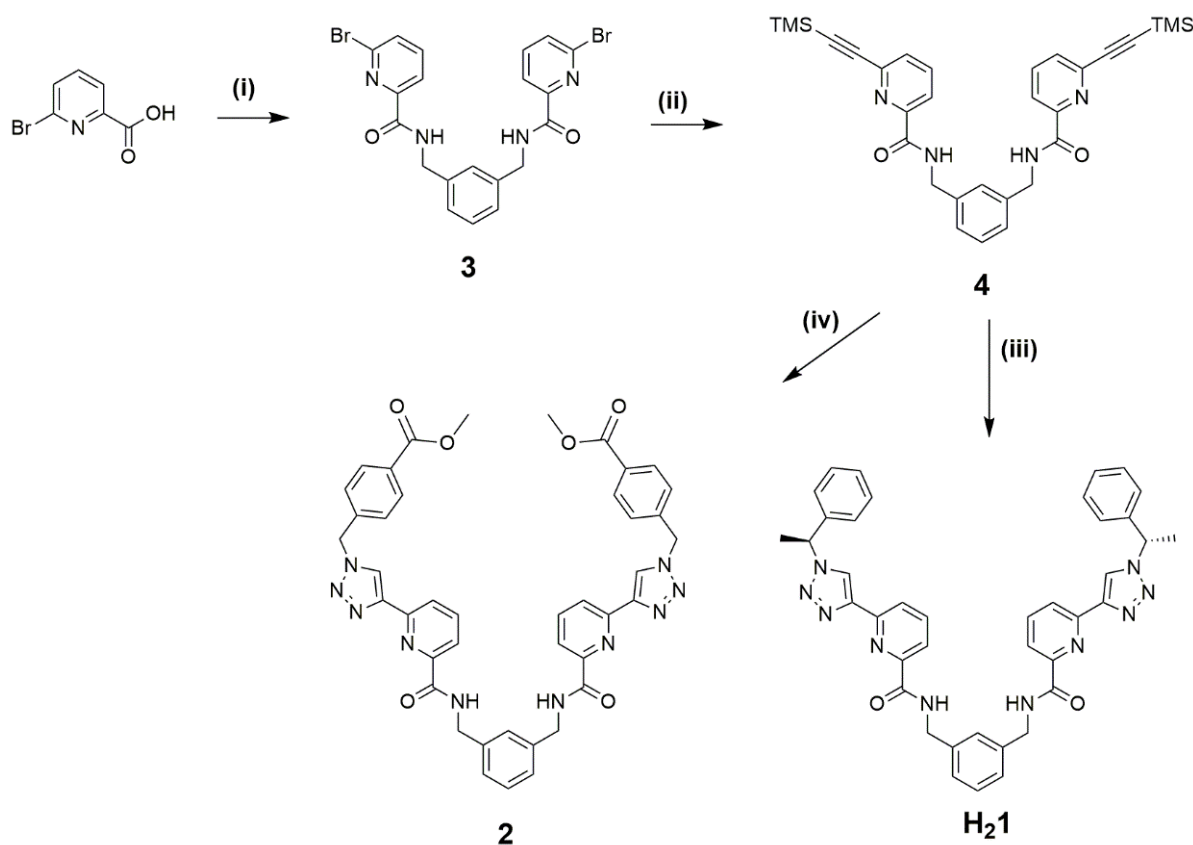
Scheme S1 *Synthesis and structure of **H$_2$1** and **2**. Reagents and conditions: (i) m-xylylenediamine, HOBt, EDCI·HCl, NEt$_3$, 4:1 DCM:DMF (ii) CuI, Pd(PPh$_3$)$_4$, TMS-acetylene, THF:NEt$_3$, (iii) (a) s-α-methylbenzylamine, ImSO$_2$N$_3$.H$_2$SO$_4$, K$_2$CO$_3$, CuSO$_4$·5H$_2$O, MeOH, (b) Na ascorbate, K$_2$CO$_3$, H$_2$O: ^{t}BuOH, **4**, DMF (iv) methyl 4-bromomethylbenzoate, NaN$_3$ CuSO$_4$·5H$_2$O, K$_2$CO$_3$, sodium ascorbate.*

Synthesis

α,α′m-Xylylenebis(N-(6-bromopicolinamide)) (3)

1,3-xylylenediamine (0.89 mL, 6.8 mmol) HOBt (1.80 g, 13.30 mmol) and NEt_3 (2.06 mL, 14.0 mmol) were added to a solution of 6-bromopyridine-2-carboxylic acid (3.00 g, 14.8 mmol) in DMF : DCM (4:1, 120 mL) under argon. The reaction mixture was stirred for 30 mins and cooled to 0 °C. EDCI·HCl (3.88 g, 20.3 mmol) was then added to the suspension and stirred at 0 °C for a further 30 mins. The mixture was then allowed to warm to room temperature and stirred for a further 48 hrs. The solvent was removed under reduced pressure and the resulting orange oil was taken up in DCM. The solution was washed with 1.0 M HCl (3×20 mL), sat. aq. $NaHCO_3$ (3×20 mL), H_2O and brine. The organic layer was dried over $MgSO_4$ and the solvent was removed under reduced pressure to yield a white solid. Yield (2.915 g, 5.78 mmol, 86 %); m.p. 168 – 171 ºC; HRMS (*m/z*) (ESI+): $C_{20}H_{16}N_4O_2Br_2Na^+$ *m/z* = 524.9538 [M+H]$^+$. Found *m/z* = 524.9531; ^{1}H NMR (400 MHz, CDCl$_3$): δ (ppm) = 8.18 (dd, 2H, pyridine H), 8.16 (br s, 2H, NH), 7.71 (t, 2H, pyridine H), 7.60 (dd, 2H, pyridine H), 7.33-7.30 (m, 4H, benzyl H), 4.63 (d, 4H, CH$_2$); ^{13}C NMR (150 MHz, CDCl$_3$): δ (ppm) = 162.5, 150.8, 140.5, 139.7, 138.4, 130.6, 129.1, 127.3, 127.2, 121.4, 43.4; IR ν_{max} (cm^{-1}): 3492, 2958, 1671, 1564, 1517, 1442, 1303, 1249, 1172, 1077, 993, 841, 760, 700, 644, 625, 622

α,α'-m-Xylenebis(N-(6-(trimethylsilylethynylpicolinamide)) (4)

To a solution of **3** (2.57 g, 5.10 mmol) in THF/NEt$_3$ stirring at 0 °C (4:1, 40 mL), CuI (0.039g, 0.2 mmol) and Pd(PPh$_3$)$_4$ (0.23 g, 0.2 mmol) were added under an argon atmosphere. Ethynyltrimethylsilane (1.6 mL, 11.22 mmol) was added dropwise and left to stir at room temperature for 48 hrs. The resulting solution was concentrated under reduced pressure and filtered through a plug of celite with DCM. The product was purified by flash column chromatography (RediSep® 24g, gradient elution $0 \rightarrow 50$ % EtOAc in Hexane) to yield a brown solid. Yield (2.469 g, 4.59 mmol, 90 %); m.p. 121 – 130 ºC; HRMS (*m/z*) (ESI+): $C_{20}H_{35}N_4O_2Si_2^+$ *m/z* = 539.2299 [M+H]$^+$. Found *m/z* = 539.2311; ^{1}H NMR (400 MHz, CDCl$_3$): δ (ppm) = 8.36 (br s, 2H, NH), 8.17 (dd, 2H, $J = 7.8$, 1.0 Hz, pyridine H), 7.81 (t, 2H, $J = 7.8$ Hz, pyridine H), 7.57 (dd, 2H, $J = 7.8$, 1.0 Hz, pyridine H), 7.34 – 7.28 (m, 4H, benzyl H), 4.66 (d, 4H, $J = 6.2$ Hz, CH$_2$), 0.27 (s, 18H, $6 \times$ CH$_3$); ^{13}C NMR (150 MHz, CDCl$_3$): δ (ppm) = 163.8, 150.1, 141.7, 138.8, 137.7, 130.1, 129.2, 127.7, 127.2, 122.0, 103.2, 96.1, 43.5, 0.2; IR ν_{max} (cm^{-1}): 3061, 2959, 1671, 1564, 1517, 1442, 1248, 1171, 1077, 993, 841, 759, 700, 644

Single crystals of the title compound were obtained from slow evaporation from hexane.

N,N'-(1,3-phenylenebis(methylene))bis(6-(1-((S)-1-phenylethyl)-1H-1,2,3-triazol-4-yl)picolinamide) (H₂1)

To a solution of (S)-α-methylbenzylamine in MeOH (0.20 mmol, 0.025 mL) was added $ImSO_2N_3 \cdot H_2SO_4$ (0.24 mmol, 60 mg) K_2CO_3 (0.40 mmol, 55 mg) and $CuSO_4 \cdot 5H_2O$ (0.04 mmol, 10 mg). The solution turned lilac after 5 hours. Then sodium ascorbate (0.09 mmol, 18 mg) and K_2CO_3 (0.02 mmol, 28 mg) were added in H_2O (0.5 mL) along with ^tBuOH (0.75 mL). The mixture was degassed with argon and turned yellow. **4** (0.11 mmol, 60 mg) was added dissolved in DMF (0.3 mL) and the reaction mixture was stirred at room temperature for 18 h. Reaction mixture was concentrated under reduced pressure and aqueous EDTA/NH₄OH (1:9, pH 9) solution was added. The product was extracted into CH_2Cl_2 and washed with H_2O (3 × 30 mL). The solution was dried over magnesium sulphate and the solvent was removed under reduced pressure to yield a white solid (48 mg, 0.012 mmol, 62 %). m.p. 118 – 123 ℃; HRMS (*m/z*) (ESI+): $C_{40}H_{37}N_{10}O_2^+$ *m/z* = 689.3101 [M+H]⁺. Found *m/z* = 689.3109; ¹H NMR (600 MHz, DMSO-*d₆*): δ (ppm) = 9.41 (t, 2H, NH), 8.98 (s, 2H, triazolyl H), 8.18 (dd, *J* = 7.8, 1.0 Hz, 2H, pyr CH-triazole), 8.02 (t, 2H, *ortho* pyr CH), 7.91 (dd, *J* = 7.7, 1.0 Hz, 2H, pyr CH-Ar), 7.45 – 7.09 (m, 14H, Ar CH), 6.05 (q, *J* = 7.1 Hz, 2H, *CH*-CH₃), 4.55 (d, *J* = 6.5 Hz, 4H, CH₂), 1.95 (d, *J* = 7.1 Hz, 6H, CH₃); ¹³C NMR (150 MHz, DMSO-*d₆*): δ (ppm) = 163.75, 149.53, 148.78, 146.79, 140.98, 139.59, 138.79, 128.82, 128.37, 128.05, 126.09, 125.61, 123.03, 121.57, 120.73, 64.90, 59.51, 42.28, 21.29; IR ν$_{max}$ (cm⁻¹): 3326, 2934, 2165, 1664, 1660, 1518, 1444, 1241, 1172, 1076, 995, 830, 765, 697

Preparation of Complexes

Cu₄(H₂1)₄ (NO₃)₈

To a solution of $Cu(NO_3)_2 \cdot 2.5H_2O$ (0.02 mmol, 3 mg) in MeOH (2 mL) was added a solution of **H₂1** (0.007 mmol, 5 mg) in MeOH (3 mL). Upon reaction together, a pale blue solution resulted and allowed to react in a closed vessel in the fridge, to yield blue crystals after one week. The crystals were isolated by filtration, washed with MeOH and allowed to air dry. Yield; (3 mg, 48%); m.p. (decomp) >280 ℃; Elemental analysis for $C_{160}H_{144}Cu_4N_{48}O_{32} \cdot 2CH_3OH$ Calculated: C 54.52 H 4.29 N 18.84; Found: C 54.22 H 3.90 N

19.13 %; IR ν_{max} (cm^{-1}): 2931, 2850, 1659, 1609, 1563, 1523, 1437, 1382, 1302, 1251, 1105, 1041, 832, 756, 696

[Cu$_4$(H1)$_4$](PF$_6$)$_4$

To a solution of [(MeCN)$_4$Cu]PF$_6$ (3 mg) in MeOH (2 mL) was added a solution of **H$_2$1** (0.007 mmol, 5 mg) in MeOH (3 mL). Upon reaction together a clear solution resulted which was subjected to vapour diffusion of toluene in the fridge, yielding blue crystals within several weeks. The crystals were isolated by filtration, washed with MeOH and allowed to air dry. Yield (2.6 mg, 40 %); m.p. (decomp) >280 ℃; Elemental analysis for C$_{160}$H$_{140}$N$_{40}$O$_8$Cu$_4$P$_4$F$_{24}$·4PhMe·12H$_2$O Calculated: C 54.14 H 4.74 N 13.43; Found: C 54.29 H 4.21 N 13.55%; IR ν_{max} (cm^{-1}): 2922, 1654, 1596, 1459, 1379, 1202, 1109, 832, 761, 734, 697, 594, 556

[Cu$_2$(H$_2$1)(NO$_3$)$_4$]MeCN

To a solution of Cu(NO$_3$)$_2$ (4 mg) in MeCN (2 mL) was added a solution of **H$_2$1** (7.0 × 10^{-3} mmol, 5 mg) in MeCN (3 mL). Upon reaction together, a pale blue solution resulted which was reacted in a closed vial for 2 days to yield blue crystals. The crystals were isolated by filtration, washed with MeCN and allowed to air dry. Yield (4 mg, 52 %); Elemental analysis for C$_{40}$H$_{36}$N$_{14}$O$_{14}$Cu$_2$·1.5 CH$_3$CN Calculated: C 45.89 H 3.63 N 19.29; Found: C 46.20 H 3.39 N 19.13%; IR ν_{max} (cm^{-1}): 3093, 1638, 1605, 1552, 1489, 1393, 1327, 1285, 1211, 1041, 1008, 830, 763, 608.

X-ray Crystallography

Data and refinement parameters are provided in Table S1. The diffraction data were collected using a Bruker APEX-II Duo dual-source instrument equipped with microfocus Cu Kα (λ = 1.54178 Å) radiation. Datasets were collected using ω and φ scans with the samples immersed in Paratone-N oil and maintained at a constant temperature of 100 K using a Cobra cryostream. The data were reduced and processed using the Bruker APEX suite of programs[S1] and multi-scan absorption corrections were applied using SADABS.[S2] The diffraction data were solved using SHELXT and refined by full-matrix least squares procedures using SHELXL-2015 within the OLEX-2 GUI.[S3] The functions minimized were $\Sigma w(F^2_o - F^2_c)$, with $w = [\sigma^2(F^2_o) + aP^2 + bP]^{-1}$, where $P = [\max(F_o)^2 + 2F^2_c]/3$. All non-hydrogen atoms were refined with anisotropic displacement parameters. All hydrogen atoms were placed in calculated positions and refined with a riding model, with isotropic displacement parameters equal to either 1.2 or 1.5 times the isotropic equivalent of their carrier atoms. X-ray powder diffraction patterns were measured on a Bruker APEX II Duo duel-source instrument using microfocus Cu Kα (λ = 1.54178 Å) maintained at 100 K using a cobra cryosystem. The patterns collected were compared with the patterns from the single crystal data (also collected at 100 K) to establish phase purity of each crystalline material.

Compound **4** was refined to convergence without the need for any additional restraints or constraints. In the case of $[Cu_4(\mathbf{H_21})_4](NO_3)_8$ and $[Cu_4(\mathbf{H1})_4](PF_6)_4$, diffuse electron density within the unit cell could not be sensibly modelled; this was accounted for using the SQUEEZE routine within PLATON.[S4] In the former case, these regions included the three non-hydrogen bonding nitrate anions, which were included in the chemical formula but could not be localised based on Fourier residuals. The bulk solvation of each complex is best accounted for by supporting bulk-phase methods, as shown in the experimental section for each compound. However, due to the rapid exchange of lattice solvents with atmospheric water and the associated loss of crystallinity, the formulation of the bulk solids is not expected to be representative of the solvated crystals, and so is not provided as the formulation of the pristine single crystals themselves, which is likely to be a mixture of the crystallization solvents and waters of crystallization of the constituent metal salts. The structural models for these two complexes also required additional restraints and/or constraints to maintain sensible chemical geometries for the poorly ordered terminal phenyl groups – these were applied to minimise the data:parameter burden already present from the intrinsic chirality of these compounds. Full

details are provided in the refine_special_details sections of the combined crystallographic information file (cif).

Crystals of compound [Cu$_2$**H$_2$1**(NO$_3$)$_4$]MeCN scattered X-rays very poorly, and we did not observe any useful data beyond a resolution of 0.93 Å. Furthermore, although ligand **1** contains chiral groups at the periphery, the vast majority of the structural model of [Cu$_2$**H$_2$1**(NO$_3$)$_4$]MeCN could be modelled with good agreement in a centric space group. The poor scattering inherent from this sample meant no statistically meaningful difference between Friedel opposites was observed to justify doubling the number of model parameters by modelling this structure in an acentric space group and halving the (already low) data:parameter ratio. Indeed, attempting a solution in an acentric space group provided problematic correlations in U$_{ij}$ parameters for almost every pair of pseudo-equivalent atoms in the structure. As such, our approach is to provide a **connectivity-only model** in a centric space group for this compound, with the proviso that this model most likely does not accurately convey the orientation of the terminal chiral groups (which differ only by the orientation of a single carbon atom at each end of the molecule). AFIX, RIGU and ISOR cards were necessary to maintain the chemical geometry of the terminal groups - details are provided in the refine_special_details sections of the combined crystallographic information file (cif).

Table S1 Crystal and refinement parameters for all structures

Identification code	[Cu$_4$(**H$_2$1**)$_4$](NO$_3$)$_8$	[Cu$_4$(**H1**)$_4$](PF$_6$)$_4$	**4**	[Cu$_2$**H$_2$1**(NO$_3$)$_4$]MeCN
Empirical formula	C$_{160}$H$_{146}$Cu$_4$N$_{48}$O$_{33}$	C$_{188}$H$_{172}$Cu$_4$F$_{24}$N$_{40}$O$_8$P$_4$	C$_{60}$H$_{68}$N$_8$O$_4$Si$_4$	C$_{42}$H$_{39}$Cu$_2$N$_{15}$O$_{14}$
Formula weight	3523.4	3953.69	1077.58	1104.96
Temperature/K	100(2)	100(2)	100(2)	100(2)
Crystal system	tetragonal	monoclinic	triclinic	monoclinic
Space group	*P*4$_3$	*C*2	*P*-1	*P*2$_1$/*c*
a/Å	23.6571(7)	36.3689(12)	11.7552(4)	24.6908(16)
b/Å	23.6571(7)	30.0761(11)	13.6950(4)	12.2647(6)
c/Å	31.1834(11)	26.1089(9)	20.8774(6)	15.4847(8)
α/°	90	90	102.4020(10)	90
β/°	90	131.776(2)	98.165(2)	97.288(5)
γ/°	90	90	106.5800(10)	90
Volume/Å^3	17452.1(12)	21297.9(14)	3070.98(17)	4651.3(5)
Z	4	4	2	4
ρ$_{calc}$g/cm^3	1.341	1.233	1.165	1.578
μ/mm^{-1}	1.254	1.422	1.297	1.857
F(000)	7288	8144	1144	2264
Crystal size/mm^3	0.18 × 0.16 × 0.06	0.24 × 0.14 × 0.1	0.6 × 0.12 × 0.04	0.14 × 0.08 × 0.03
Radiation	CuKα (λ = 1.54178)	CuKα (λ = 1.54178)	CuKα (λ = 1.54178)	CuKα (λ = 1.54178)
2Θ range for data collection/°	6.79 to 136.834	6.518 to 136.874	4.44 to 139.826	3.608 to 113.816
Index ranges	-27 ≤ h ≤ 27, -28 ≤ k ≤ 27, -37 ≤ l ≤ 37	-43 ≤ h ≤ 43, -35 ≤ k ≤ 36, -31 ≤ l ≤ 31	-14 ≤ h ≤ 14, -16 ≤ k ≤ 16, -24 ≤ l ≤ 25	-26 ≤ h ≤ 26, -13 ≤ k ≤ 13, -15 ≤ l ≤ 16
Reflections collected	88981	114816	35417	49115
Independent reflections	31736 [R$_{int}$ = 0.0576, R$_{sigma}$ = 0.0686]	38707 [R$_{int}$ = 0.0481, R$_{sigma}$ = 0.0544]	11490 [R$_{int}$ = 0.0515, R$_{sigma}$ = 0.0505]	6255 [R$_{int}$ = 0.2490, R$_{sigma}$ = 0.1285]
Reflections Observed [I>=2σ (I)]	22806	33716	10172	3859
Data/restraints/parameters	31736/112/2083	38707/412/2551	11490/0/697	6255/264/635
Goodness-of-fit on F^2	1.011	1.033	1.054	1.049
Final R indexes [I>=2σ (I)]	R$_1$ = 0.0752, wR$_2$ = 0.2006	R$_1$ = 0.0671, wR$_2$ = 0.1880	R$_1$ = 0.0571, wR$_2$ = 0.1572	R$_1$ = 0.1298, wR$_2$ = 0.2913
Final R indexes [all data]	R$_1$ = 0.1002, wR$_2$ = 0.2343	R$_1$ = 0.0747, wR$_2$ = 0.1998	R$_1$ = 0.0616, wR$_2$ = 0.1640	R$_1$ = 0.1847, wR$_2$ = 0.3186
Largest diff. peak/hole / e Å^{-3}	0.62/-0.71	0.81/-0.38	0.92/-0.46	1.04/-0.63
Flack Parameter	-0.008(18)	0.012(7)	n/a	n/a
CCDC No.	1905243	1905244	1905245	1905246

Structure of Compound 4

The diffraction data for **4** were solved and refined in the triclinic space group *P*-1, where the asymmetric unit contains two complete molecules of the title compound and no solvent or guest species. The two unique species adopt slightly different conformations of the amide groups about the central xylyl bridge, but both adopt relatively similar U-shaped conformations as a whole. Strong association is evident by way of intermolecular hydrogen bonding from the four amide N-H groups – each of these interactions serves to bind the two residues into a tight dimer. Two hydrogen bonding modes are evident; amide nitrogen atoms N4 and N6 each donate hydrogen bonds to the pyridine nitrogen atom of their opposite residue, with N···N distances 3.162(2) and 3.249(2) Å, respectively, and N-H···N angles of 160.6° and 163.13°, respectively. The other interactions are accounted for through intermolecular amide-amide hydrogen bonding originating from nitrogen atoms N2 and N8. These show N···O distances of 2.957(2) and 2.930(2) Å, respectively, and N-H···O angles of 134.5° and 137.0°, respectively, with closer or more linear association being prohibited by the steric clashes between the folded **4** molecules. Interactions between the π systems of the xylyl and pyridyl rings of the two molecules within the dimer are also evident, with the closest interatomic distance of 3.373(2) Å for C5···N5 being typical for a heterotopic π-π interaction (the mean interplanar angle is approximately 9°). With all of the strong hydrogen bond donors being accounted for in the dimerization of these species, the remaining intermolecular interactions between adjacent dimers consists largely of π-π, C-H···π and C-H···O interactions, leading to a densely packed structure. The structure and primary hydrogen bonding interactions in **4** are shown in Figure S1.
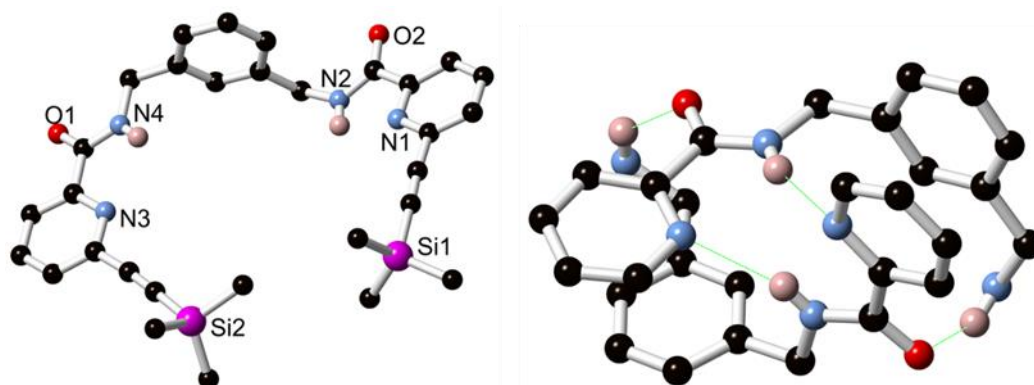
Figure S1 *(Left) Structure of one unique molecule of compound **4** with heteroatom labelling scheme. Selected hydrogen atoms are omitted for clarity. (Right) Primary mode of interaction between the two species in the solid-state **4** dimer. Terminal trimethylsilyl-alkynylpyridine groups and selected hydrogen atoms are omitted for clarity.*

Structure of [Cu$_2$(H$_2$1)(NO$_3$)$_4$]·MeCN

Single crystals of the title compound were analysed by single crystal X-ray diffraction. Although the diffraction data were not of sufficient quality to distinguish the Friedel pairs and resolve the handedness of the terminal chiral centres (as discussed in the X-ray crystallography section), a connectivity model could nonetheless be refined in the monoclinic space group $P2_1/c$. In this centric model (shown in Figure S2), the asymmetric unit contains one molecule of the discrete dinuclear complex [Cu$_2$(**H$_2$1**)(NO$_3$)$_4$], and one lattice acetonitrile molecule. This complex bears strong similarities to the discrete dinuclear species observed from our previous achiral **tzpa** ligand, and so will not be discussed in great depth. The two unique copper ions adopt similar coordination geometries, both displaying square pyramidal coordination spheres with the tridentate (N,N,O) ligand and one monodentate nitrato ligand occupying the basal plane and the axial position occupied by a second monodentate nitrato anion. Both sites show little tendency towards trigonal bipyramidal geometry (τ_5 = 0.06 and 0.14 for Cu1 and Cu2, respectively),[S5] and the axial nitrato ligands show elongated Cu-O bonds (*ca.* 2.2 – 2.3 Å) compared to those in the equatorial plane (*ca.* 1.9 – 2.0 Å).

The ligand adopts a compact folded conformation about the central *m*-xylyl group which imparts a Cu-Cu distance of 8.56 Å. This conformation is supported by intramolecular hydrogen bonding interactions from the amide groups of the ligand to the non-coordinating nitrato oxygen atoms from the adjacent binding pocket. Beyond these interactions, only diffuse crystal packing interactions are evident in the extended structure, with offset face-to-face π-π interactions forming the most obvious of these contacts. The terminal chiral arms do not undergo any specific or directional intermolecular interactions with nearby molecules; most likely the lack of any strong interactions with these side chains is related to the predominantly centric character of the structure as a whole.
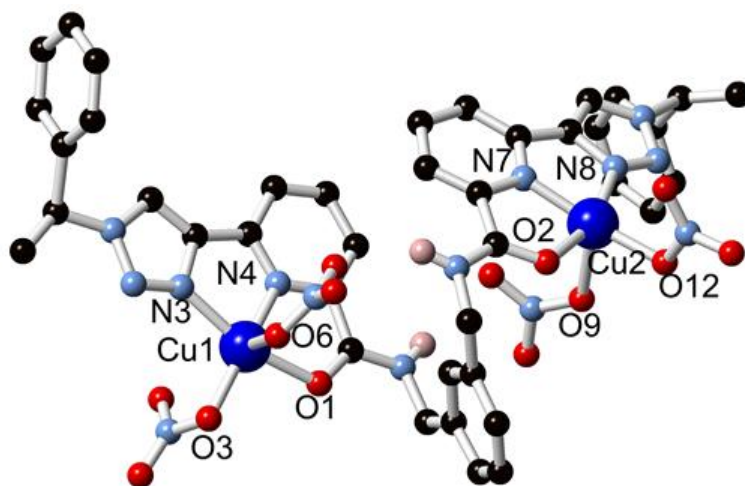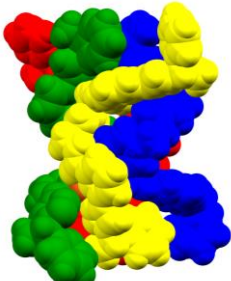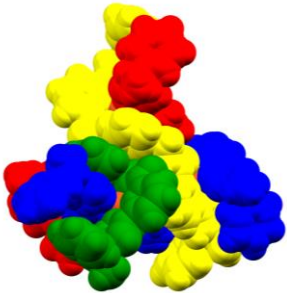
Figure S2 *Structure of [Cu₂(**H₂1**)(NO₃)₄]·MeCN modelled in the centric space group P2₁/c with labelling scheme for unique heteroatoms. Selected hydrogen atoms and lattice acetonitrile molecule are omitted for clarity.*

Table S2 *Comparison of the geometric parameters for [Cu₄(**H₂1**)₄](NO₃)₈ and [Cu₄(**H1**)₄](PF₆)₄*

	[Cu₄(**H₂1**)₄](NO₃)₈	Compound	[Cu₄(**H1**)₄](PF₆)₄	
	10.83	d_{avg}Cu-Cu (Intrastrand, Å)	8.77	
	8.20	d_{avg}Cu-Cu (interstrand, Å)	10.33	
	2310	Molecular Volume (Å³)	2292	
	102	Cu₄ tetrahedral volume (Å³)	86	
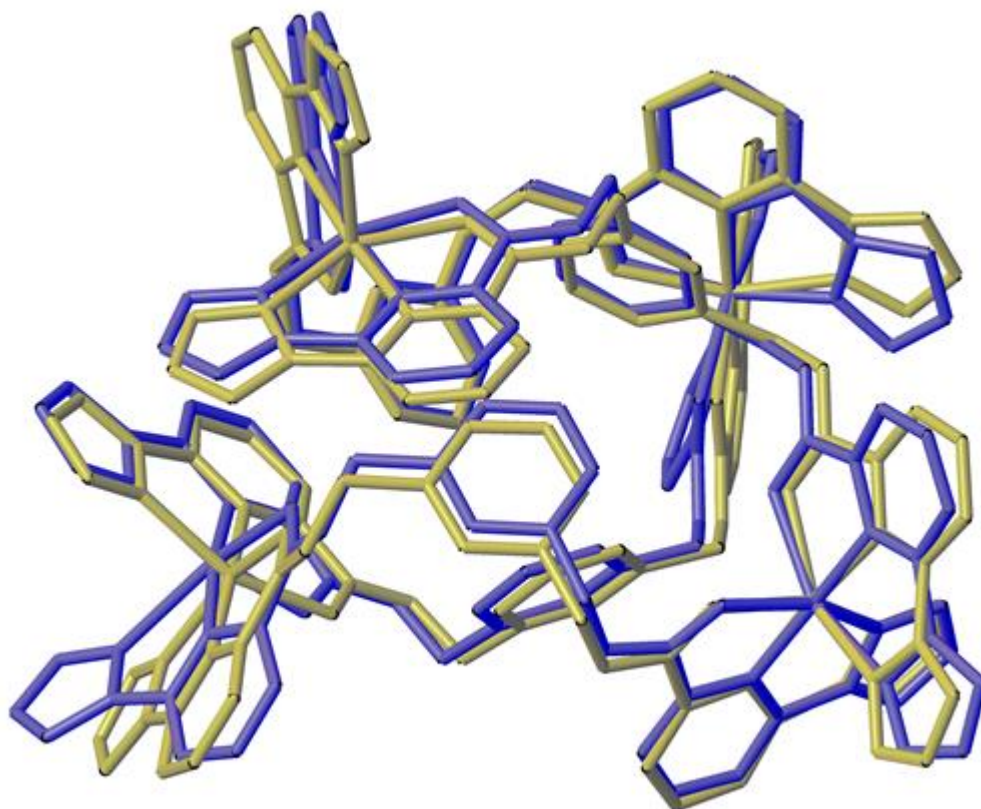
Figure S3 *Overlay of complex [Cu$_4$(**H$_2$1**)$_4$](NO$_3$)$_8$ (blue) with the tetranuclear zinc complex reported by Barry et al.[S6] (grey), showing the overlap of the four metal sites (used as anchor points) and the close similarity in ligand folding. Side arms, lattice solvents, anions and hydrogen atoms are omitted for clarity.*

Additional UV-visible and Fluorescence Spectra
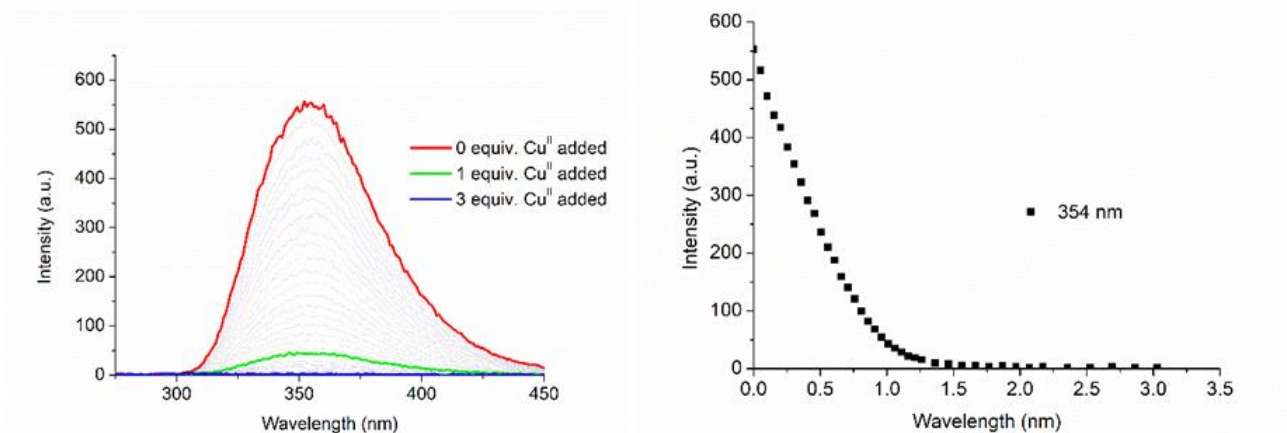
Figure S4 *(Left) overall changes to the fluorescence spectra upon titrating* **H₂1** *(1 x 10⁻⁵ M) against Cu(NO₃)₂ (0 – 3 equiv.) in MeOH at RT. (Right) corresponding experimental binding isotherm at λ = 354 nm*
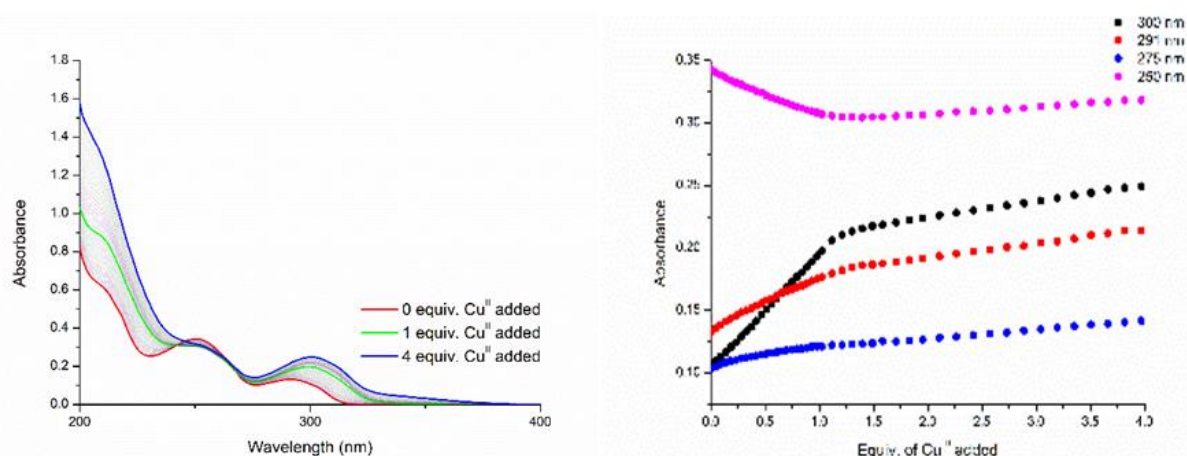
Figure S5 *(Left) The overall changes in the UV-visible absorption spectra upon titrating* **H₂1** *(1 x 10⁻⁵ M) against Cu(NO₃)₂ (0 – 4 equiv.) in MeCN at RT. (Right): corresponding experimental binding isotherms of absorbance at λ = 250, 275, 291 and 300 nm.*
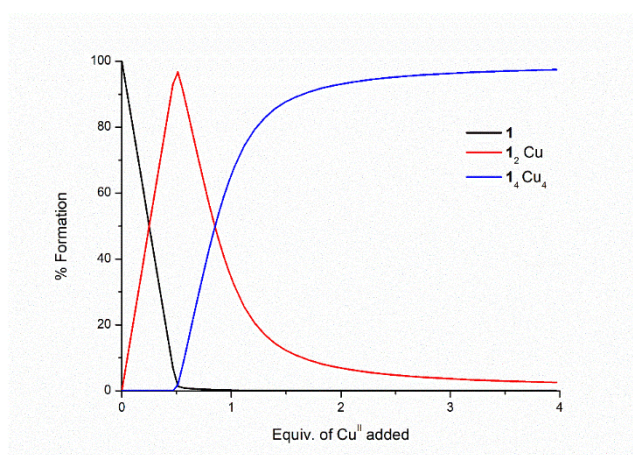
Figure S6 *Speciation distribution diagram of Cu(NO₃)₂ species in MeCN obtained from UV-visible absorption titration data fit*
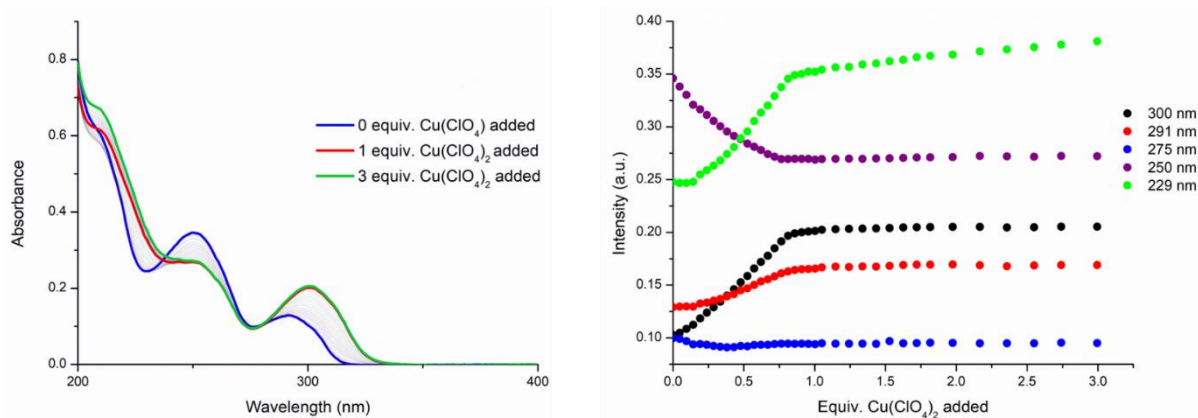
Figure S7 *(Left) overall changes to the UV-visible absorption spectra upon titrating **$H_2 1$** (1 x 10^{-5} M) against Cu(ClO$_4$)$_2$ (0 – 3 equiv.) in MeCN at RT (Right) corresponding experimental binding isotherms of absorbance at λ = 229, 250, 275, 291 and 300 nm*
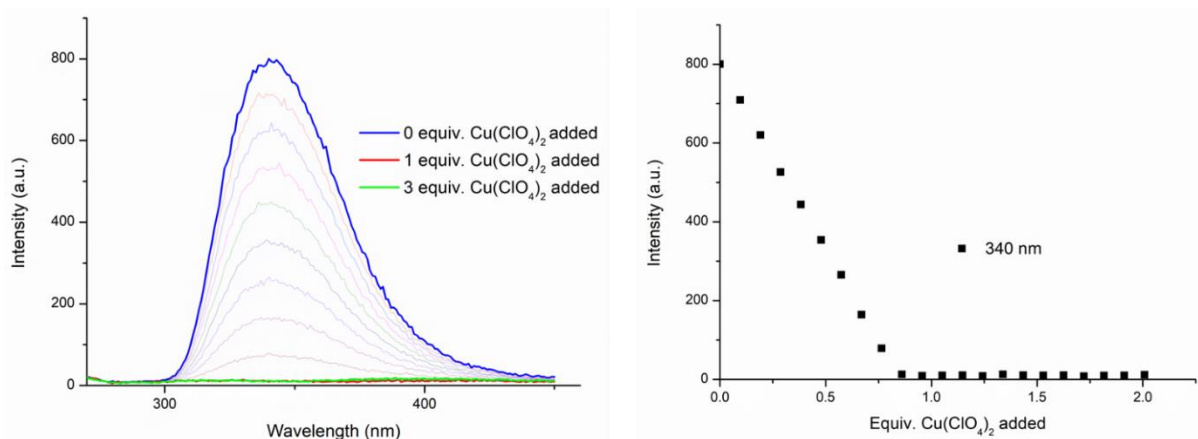
Figure S8 *(Left) overall changes to the fluorescence spectra upon titrating **$H_2 1$** (1 x 10^{-5} M) against Cu(ClO$_4$)$_2$ (0 – 3 equiv.) in MeCN at RT. (Right) corresponding experimental isotherm at λ = 340 nm*
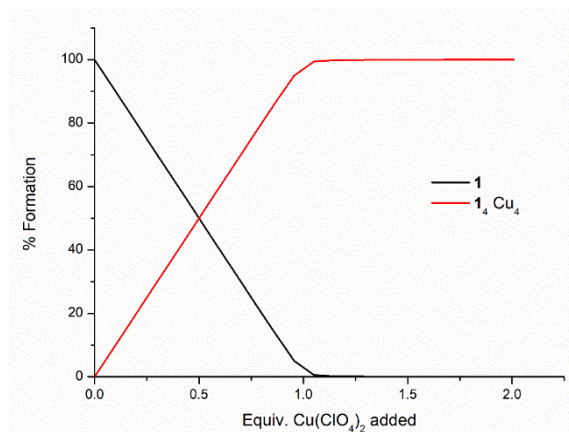
Figure S9 *Speciation distribution diagram of Cu(ClO$_4$)$_2$ obtained from UV-visible absorption titration data fit*
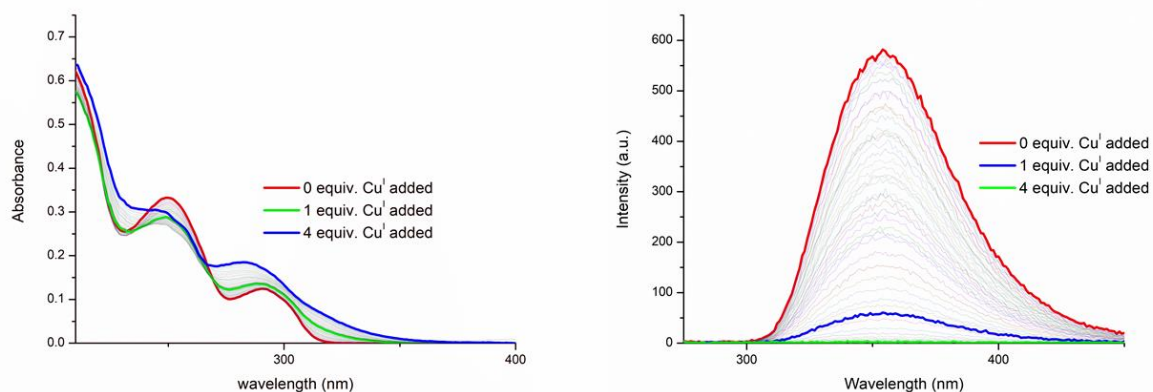
Figure S10 *(Left) overall changes to the UV-visible absorption spectra upon titrating H_2I (1 x 10^{-5} M) against [Cu(MeCN)$_4$](PF$_6$) (0 – 4 equiv.) in MeCN at RT (Right) overall changes to the fluorescence spectra upon titrating H_2I (1 x 10^{-5} M) against [Cu(MeCN)$_4$](PF$_6$) (0 – 4 equiv.) in MeCN at RT.*
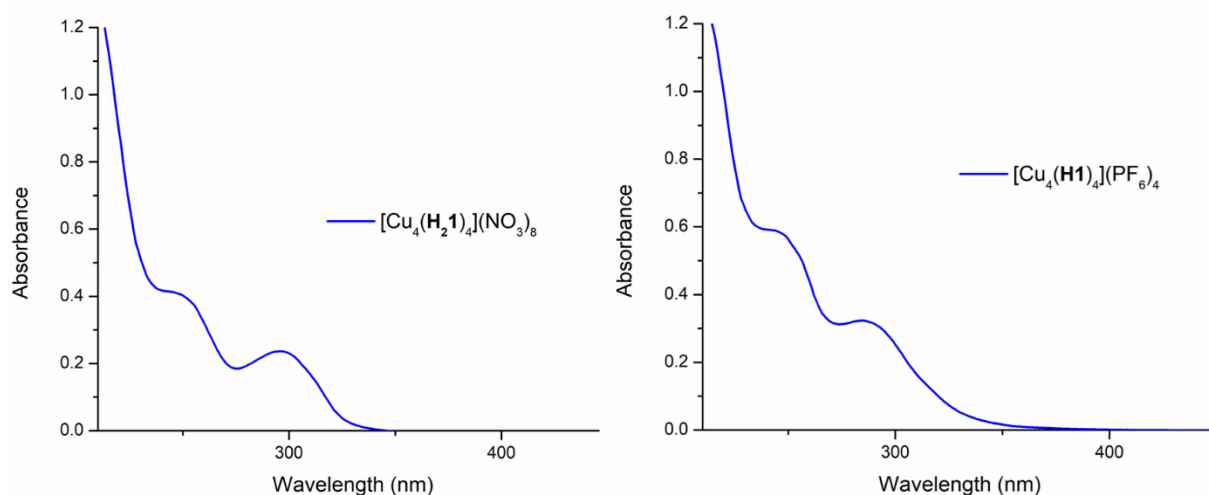
Figure S11 *UV-vis absorbance spectra of (Left) [Cu$_4$(H_2I)$_4$](NO$_3$)$_8$ and (right) [Cu$_4$($H1$)$_4$](PF$_6$)$_4$ recorded in MeOH (approx. 1.1×10^{-5} M)*
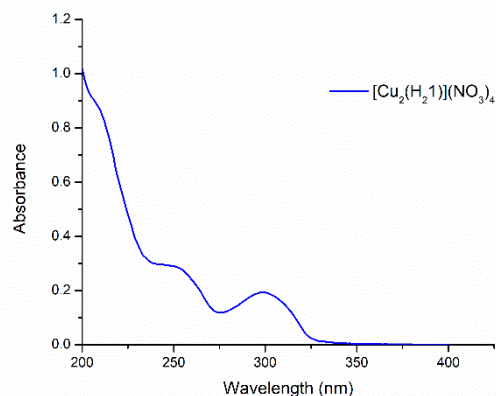
Figure S12 *UV-vis absorbance spectrum of [Cu$_2$(H_2I)](NO$_3$)$_2$ recorded in MeCN (approx. 1.1×10^{-5} M)*
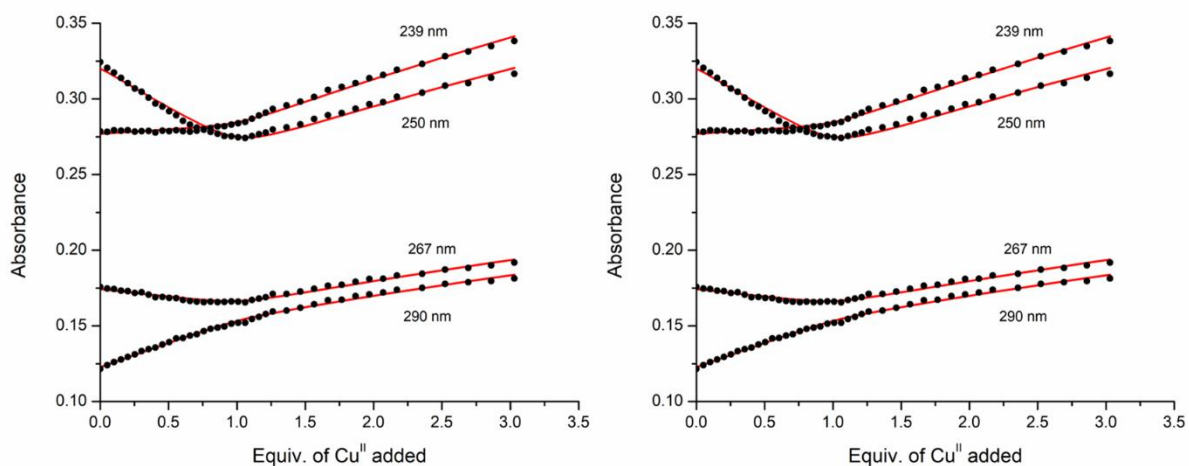
Figure S13 *Fit of experimental binding isotherms using non-linear regression analysis program ReactLab Equilibria of ligand **$H_2$1** with (left) Cu(NO₃)₂ in MeOH and (right) Cu(NO₃)₂ in MeCN*
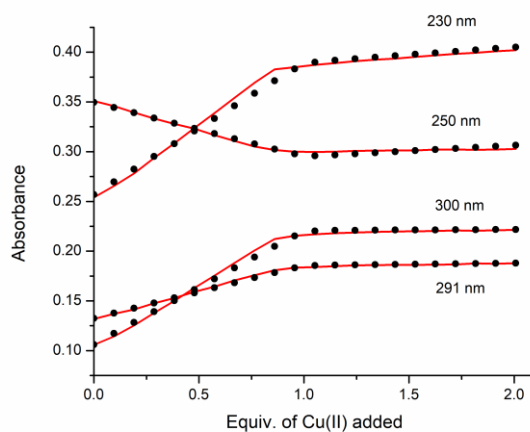
Figure S14 *Fit of experimental binding isotherms using non-linear regression analysis program ReactLab Equilibria of ligand **$H_2$1** with Cu(ClO₄)₂ in MeCN*
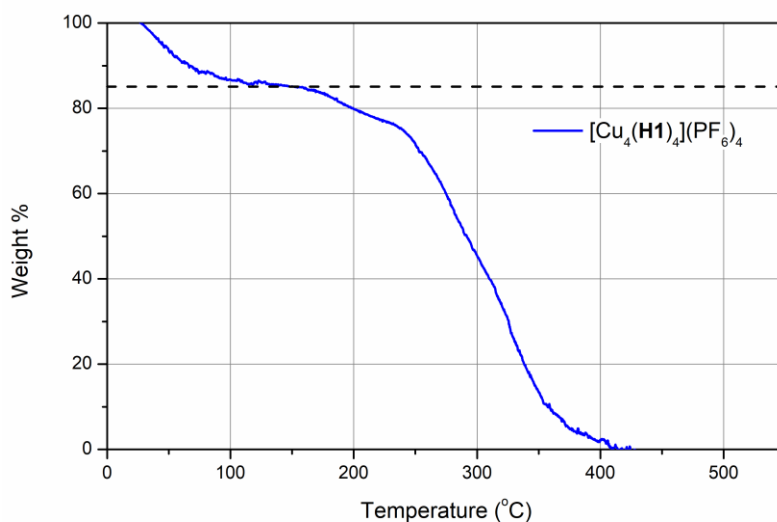
Figure S15 *Thermogravimetric analysis plot of [Cu₄(**H1**)₄](PF₆)₄ which shows loss of H₂O and PhMe*

X-Ray Powder Diffraction
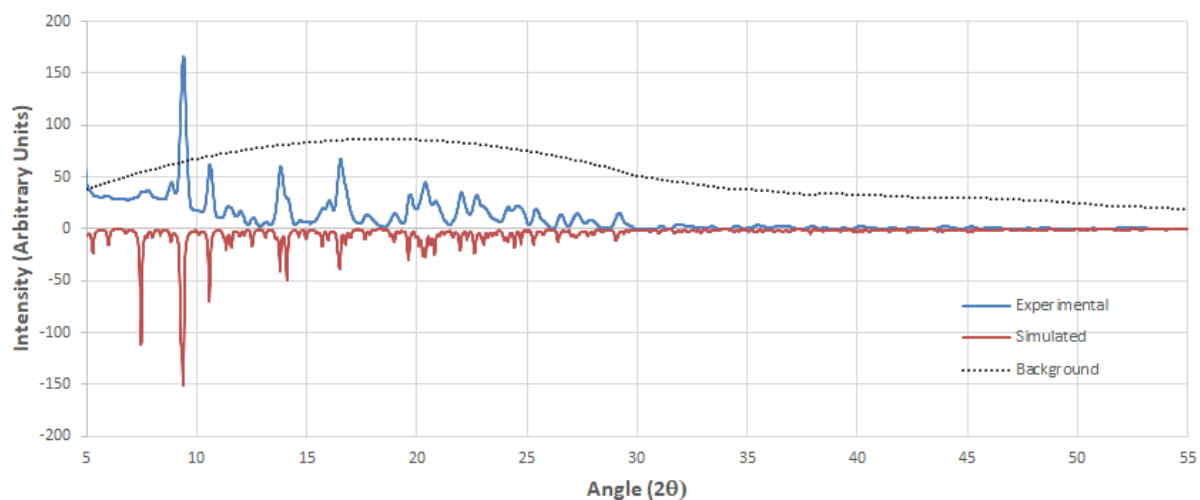
Figure S16 *X-ray diffraction pattern for Cu$_4$(**H$_2$1**)$_4$(NO$_3$)$_8$ measured at (100 K) (blue) compared to the pattern simulated from the single crystal X-ray data obtained at (100K) (red)*
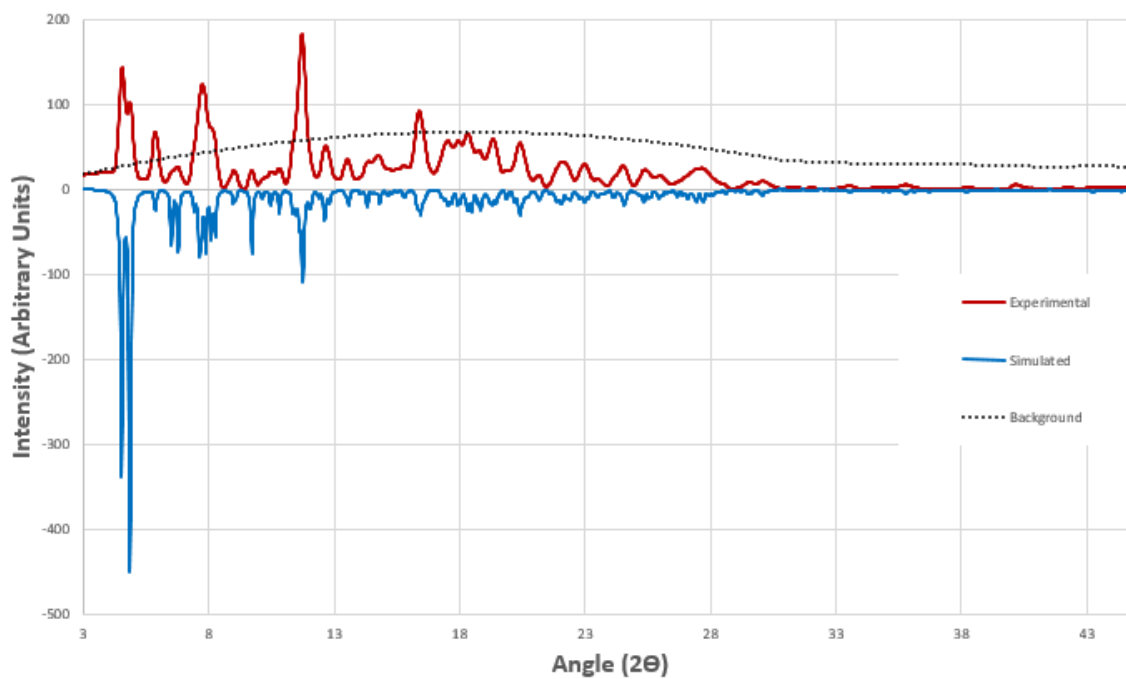
Figure S17 *X-ray diffraction pattern for Cu$_4$(**H1**)$_4$ PF$_6$ measured at (100 K) (red) compared to the pattern simulated from the single crystal X-ray data obtained at (100K) (blue)*
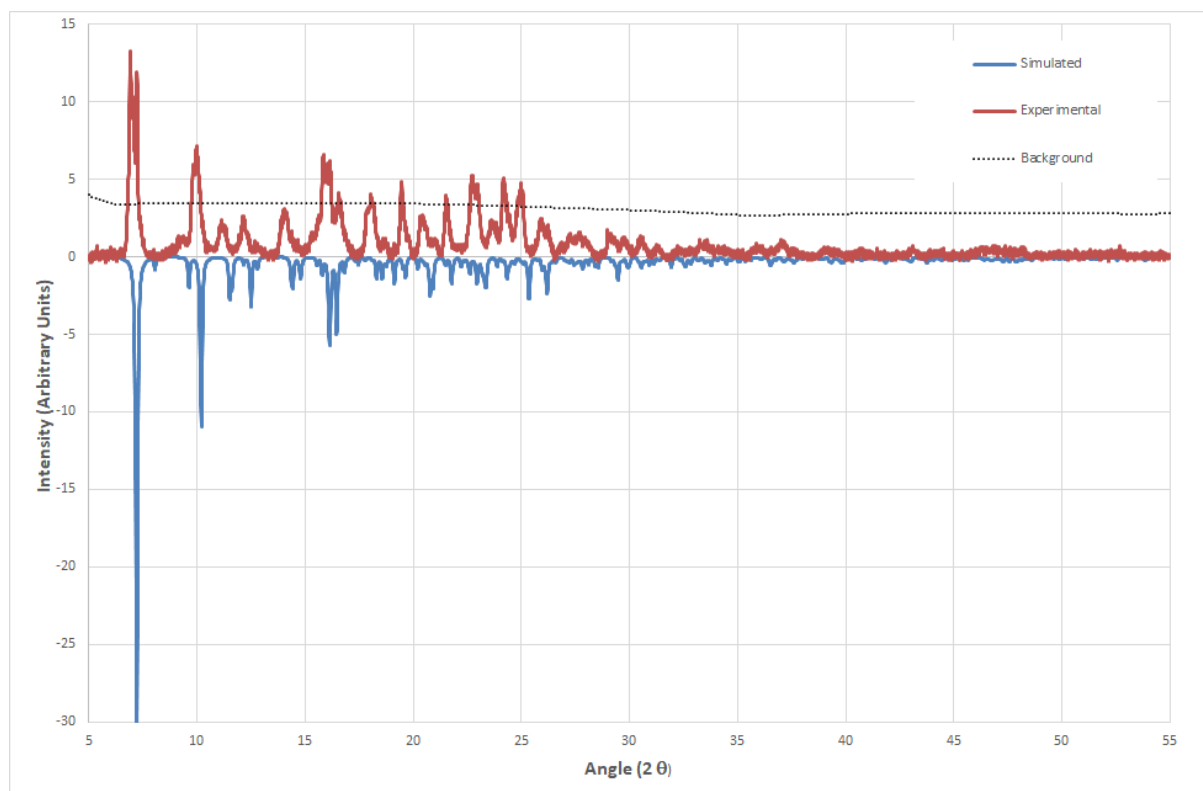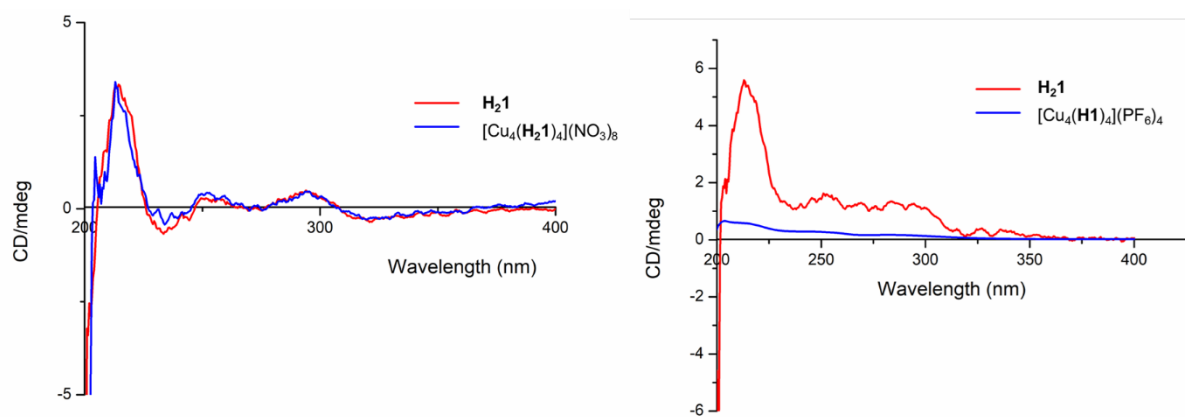
Figure S18 *X-ray diffraction pattern for [Cu₂(**H₂1**)(NO₃)₄]MeCN measured at (100 K) (red) compared to the pattern simulated from the single crystal X-ray data obtained at (100K) (blue)*

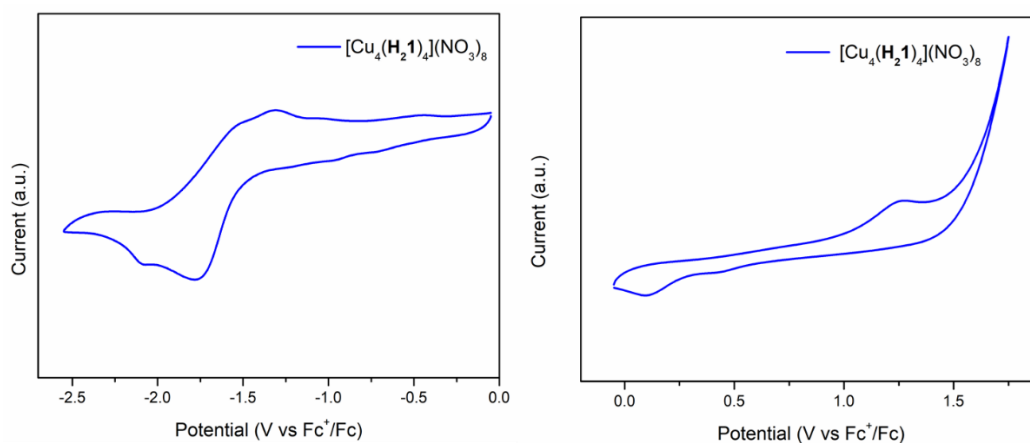**Figure S19** *The CD spectra of **H₂1** (1×10⁻⁵M) along with 1 equiv. of (left) Cu(NO₃)₂ and (right) [Cu(MeCN)₄](PF₆) in MeOH at 25 ˚C*

Figure S20 *Cyclic voltammetry of (left) anodic and (right) cathodic traces of $[Cu_4(\mathbf{H_2 1})_4](NO_3)_8$ recorded in deaerated acetonitrile; supporting electrolyte TBAPF$_6$ 0.1 M. The Fc$^+$/Fc couple was used as an internal standard. Scan rates were at 100 mV s^{-1}*
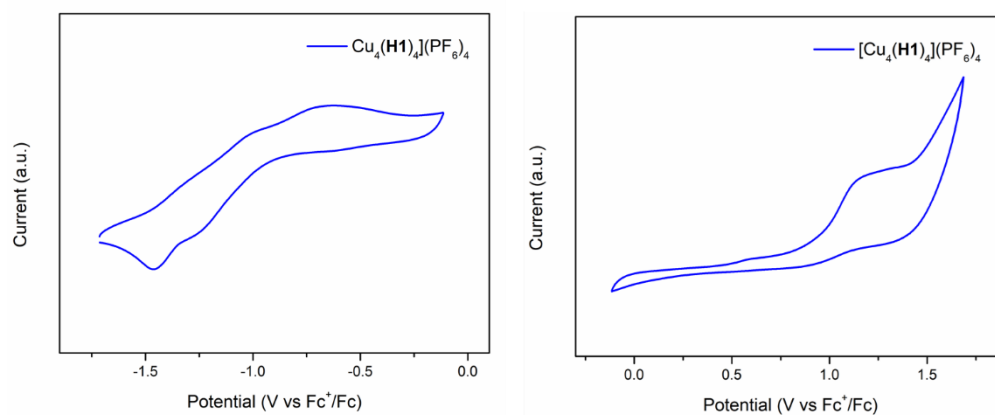

Figure S21 *Cyclic voltammetry of (left) anodic and (right) cathodic traces of $[Cu_4(\mathbf{H1})_4](PF_6)_4$ recorded in deaerated acetonitrile; supporting electrolyte TBAPF$_6$ 0.1 M. The Fc$^+$/Fc couple was used as an internal standard. Scan rates were at 100 mV s^{-1}*
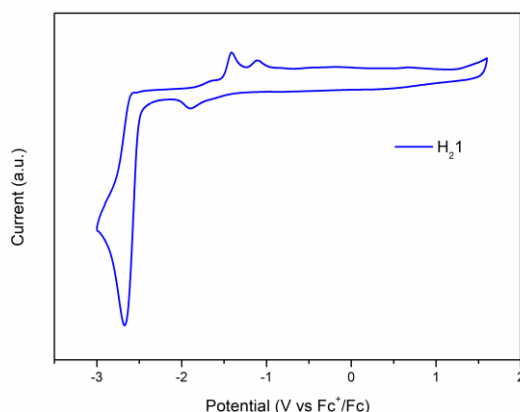

Figure S22 *Cyclic voltammetry of H$_2$1 recorded in deaerated acetonitrile; supporting electrolyte TBAPF$_6$ 0.1 M. The Fc$^+$/Fc couple was used as an internal standard. Scan rate was at 100 mV s^{-1} in the negative direction.*
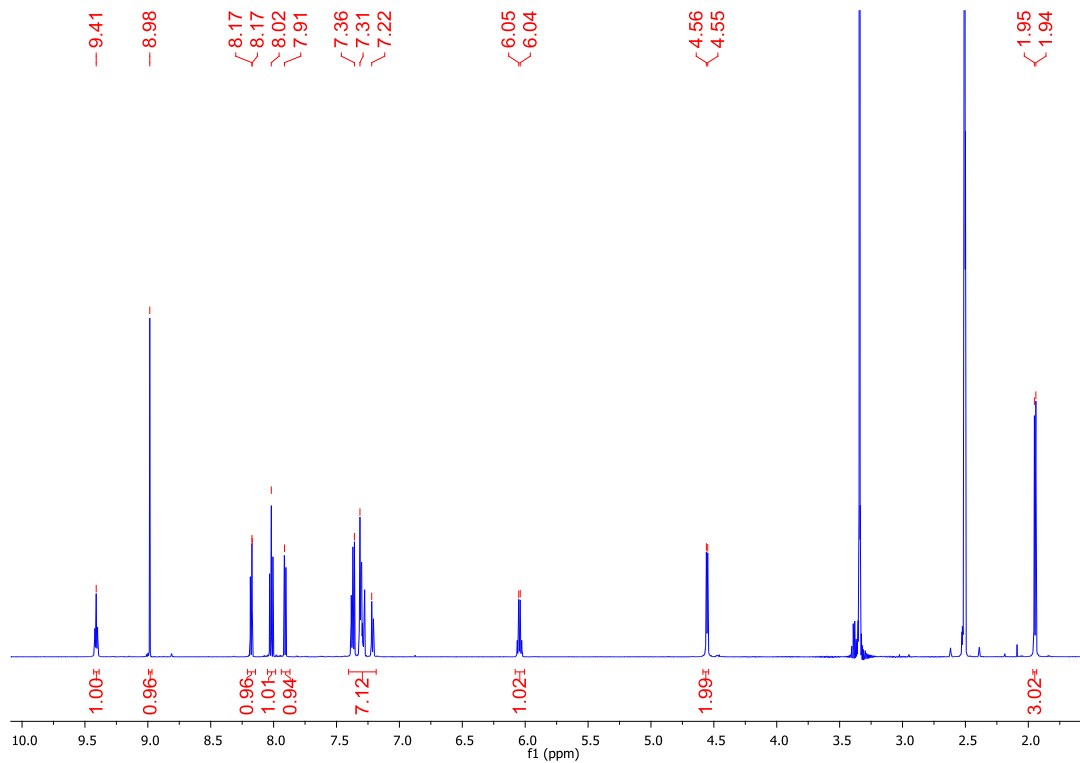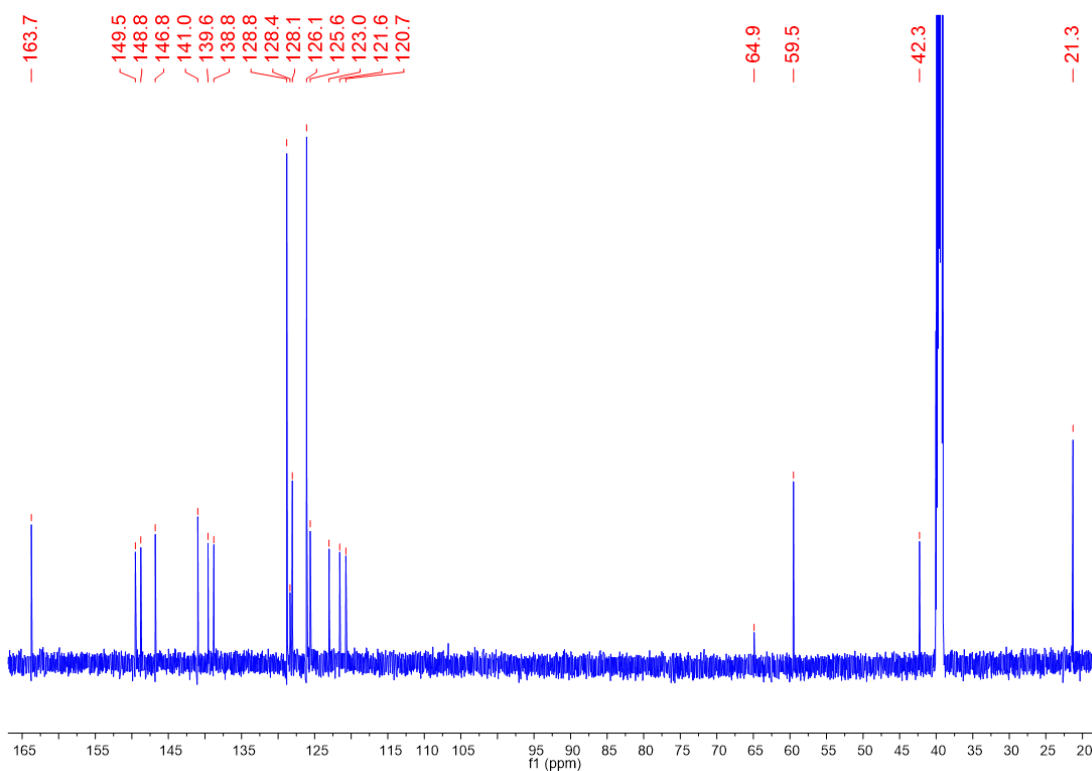
Figure S23 *^{1}H NMR (600 MHz, DMSO) of **H₂1** at RT.*

Figure S24 *^{13}C NMR (150 MHz, DMSO) of **H₂1** at RT.*

References

S1   APEX-3, Bruker-AXS Inc, Madison WI, 2016

S2   SADABS, Bruker-AXS Inc, Madison WI, 2016

S3   G. M. Sheldrick, *Acta Crystallogr. Sect. A*: *Found. Adv*. 2015, **71**, 3; G. M. Sheldrick, *Acta Crystallogr., Sect. C*: Struct. Chem. 2015, **71**, 3−8; O. V. Dolomanov, L. J. Bourhis, R. J. Gildea, J. A. K. Howard and H. J. Puschmann., *Appl. Crystallogr.*, 2009, **42**, 339.

S4   A. L. Spek, *Acta. Crystallogr. Sect. C: Struct. Chem.* 2015, **71**, 9-18

S5   A. W. Addison, T. N. Rao, J. Reedijk, J. van Rijn and G. C. Verschoor, *J. Chem. Soc., Dalton Trans.* 1984, 1349-1356.

S6   D. E. Barry, C. S. Hawes, J. P. Byrne, B. la Cour Poulsen, M. Ruether, J. E. O'Brien, T. Gunnlaugsson, *Dalton Trans.,* 2017, **46**, 6464-6472.